08,03

# Photoinduced changes in impedance and conductivity of $CuInSe_2$ films depending on their synthesis technology

© O.B. Romanova[1], S.S. Aplesnin[1,2], T.M. Gadzhiev[3], M.N. Sitnikov[2], M.A. Aliev[3], O.S. Nikitinsky[2], L.V. Udod[1,2]

[1] Kirensky Institute of Physics, Federal Research Center KSC SB, Russian Academy of Sciences, Krasnoyarsk, Russia
[2] Siberian State University of Science and Technology, Krasnoyarsk, Russia
[3] Amirkhanov Institute of Physics, Daghestan Federal Research Center, Russian Academy of Sciences, Makhachkala, Russia

E-mail: rob@iph.krasn.ru

*Received October 24, 2025*
*Revised October 24, 2025*
*Accepted October 25, 2025*

Using the controlled selenization method, $CuInSe_2$ films with a chalcopyrite structure were synthesized. It was established that the selenization temperature ($T_{sel}$) is a critical parameter determining the morphology and electrophysical properties of the films. A nonlinear current-voltage characteristic was found, caused by the electrical inhomogeneity of the material. The optimum $T_{sel} = 350\,^{\circ}C$ was determined, at which the maximum photoelectric effect and the longest relaxation time are observed. At $T_{sel} < 300\,^{\circ}C$, a photoinduced change in impedance was detected.

**Keywords:** polycrystalline films, electrophysical properties, photoconductivity.

DOI: 10.61011/PSS.2025.10.62643.295-25

## 1. Introduction

Polycrystalline semiconductor films $CuInSe_2$ with chalcopyrite structure are one of the essential and promising materials in production of highly efficient solar energy converters [1–4]. $CuInSe_2$ (GIS) — is a I-III-$VI_2$ semiconductor of *p*-type with a straight band gap of about 1.0 eV, which is ideal for photoelectric materials. These materials are featuring high efficiency of solar elements 22.6 % as per NREL) [5–7]. To create efficient solar cells based on $Cu(In,Ga)Se_2$ (CIGS) or LEDs, it is necessary to control defects that impair their performance. In the study [8] the major „cause" was described — anion vacancies. On the other hand, anion vacancies, due to the strong relaxation of the lattice when their charge state changes, are a universal cause of stable photoconductivity in many important semiconductor materials. A paradox is observed in $CuInSe_2$: a material with a large number of defects demonstrates record-high efficiency values for thin-film technologies (more than 20 %). The study [9] explains this paradox using modeling with ab initio analysis. The authors discuss the properties of the so-called „ordered defective phase" $CuIn_3Se_5$. They show that its „band gap" is almost the same as that of the stoichiometric $CuInSe_2$. This means that even areas with a strong deviation from stoichiometry do not create barriers to photocurrent. Based on all the above, it is important to note the distinctive feature of CIS — high tolerance to structural defects and deviations from stoichiometry. Significant concentrations of point defects (vacancies, interstitial atoms, etc.) and extended defects (grain boundaries) do not lead to catastrophic recombination of charge carriers, as in many other semiconductors (e. g., Si). This is a key property for its wide application in photovoltaics. The conductivity (type and level) is effectively controlled by the ([Cu]/[In] ratio as well as the growth/annealing conditions. With the deficiency of copper ($[Cu]/[In] < 1$) *p*-type of conductivity is enhanced, and with the excess of copper ($[Cu]/[In] > 1$) *n*-type may occur [10]. The annealing conditions in the selenium atmosphere affect selenium vacancies, and the temperature changes the mobility of defects. For example, annealing in vacuum creates vacancies V(Se) (donors), and in the atmosphere of Se — compensates for them. Growth and annealing conditions such as temperature, selenium vapor pressure, time, and atmosphere all affect the formation and concentration of point defects that determine the electrical properties of [11–13]. The forward band gap ($\sim 1.0$ eV) causes a very high light absorption coefficient ($> 10^5\,cm^{-1}$) in the visible and near-infrared spectral regions of polycrystalline $CuInSe_2$ films [14]. Despite the high defect density, electrons (non-basic carriers in *p*-type of CIS) have a relatively long diffusion length ($L_n > 1\,\mu m$) [15]. This fundamental property, along with its defective tolerance, makes CIS exceptionally suitable for thin-film solar cells. Magnetic properties do not play a role in its application, since the material is diamagnetic or weakly paramagnetic and does not exhibit any ferromagnetism. Reaching the record-hitting efficiencies ($> 23$ %) in devices based on

its solid solution CIGS attests its outstanding photovoltaic characteristics.

Another main parameter determining the completeness of the GIS phase formation reaction is grain size; defect concentration; stoichiometry — selenization temperature $T_{sel}$ [16–18]. The results of X-ray diffraction and Raman spectroscopy showed on example of thin films of $Cu_2SnSe_3$ that films deposited at lower selenization temperatures ($350-500\,^\circ C$) contained mixed phases of cubic or monoclinic $Cu_2SnSe_3$ in addition to the secondary phases $Cu_{2-x}Se$ and SnSe [19]. At low selenization temperatures, it is considered that the selenization reaction is incomplete and intermediate phases are formed. The optimal selenization temperature is considered to be $450-550\,^\circ C$, since there is a complete reaction of formation of a homogeneous crystalline phase [20] $CuInSe_2$ films have large grains $> 1\,\mu m$. This is the temperature range where the chalcoperite structure with the best electrical properties is formed. As the selenization temperature rises, the mobility of charge carriers increases in the optimal range, due to a larger grain size and an improvement in crystallinity, which leads to a decrease in scattering by lattice defects [21]. High selenization temperatures $< 550-600\,^\circ C$ are a risk of decomposition of $CuInSe_2$ system into volatile components, deterioration of morphology (melting of grains, voids), possible formation of nonstoichiometric phases or secondary phases at grain boundaries.

Despite the great practical need to study the physical properties of $CuInSe_2$, the effect of the frequency of an alternating electric field on the transport characteristics of these compounds has not been studied. Experimental studies on magnetoimpedance in $CuInSe_2$ are still an unresolved issue. Because magnetic fields can affect the mobility of current carriers and their scattering at grain boundaries. The magnetic impedance on polycrystalline $CuInSe_2$ films will depend on the selenization temperature and on grain boundaries, nonstoichiometry, and defects. Specifically, changes in Cu/In ratios (e.g., films with an excess of In) and nonstoichiometry can create defective states that affect transport characteristics in a magnetic field.

The purpose of this work was to establish the optimal selenization temperature for the synthesis of polycrystalline $CuInSe_2$ films that exhibit the maximum photoinduced change in resistance and impedance in a magnetic field.

## 2. Synthesis and measurement procedure

Thin films of $CuInSe_2$ with chalcopyrite structure were obtained by a three-stage controlled selenization method of Cu/In intermetallic precursors pre-deposited on glass substrates. Deposition was carried out on an automated magnetron system „BATT AMK-MI". A conductive disk with a diameter of 40 mm and a thickness of 4 mm was used as a target, made by fusing the initial elements Cu (99.99 at.%) and In (99.999 at.%) taken in a stoichiometric composition. To obtain high purity Cu-In-Se, the first two stages were carried out at a pressure of $p = 10^{-3}$ Pa, which minimizes possible contamination. To reduce potential evaporation of synthesized binary copper and indium selenides from the film surface, at the third stage, the pressure of the vapor-gas mixture $Se + N_2$ increased to 1 Pa. The advantages of this approach to the synthesis of polycrystalline films are the possibility of obtaining large-area layers with a homogeneous composition and the same thickness. The temperature in the reaction zone of Cu-In layers with Se (selenization temperature $T_{sel}$) varied in the range $200\,^\circ C \le T_{sel} \le 550\,^\circ C$.

Phase composition and structure properties of the grown $CuInSe_2$ films were studied using PANalytical Empyrean Series 2 X-ray diffractometer with emission wavelength (CuK$\alpha$) $\lambda = 0.15418$ nm, within the angles range $2\theta = 15 \div 60^\circ$, with the angle setting accuracy of $0.0001^\circ$, $2\Theta$ linearity $\pm 0.004^\circ$, and scanning rate $0.02^\circ$. The phases were identified by comparing experimentally determined interplanar distances with ICDD data (The International Centre for Diffraction Data).

The surface morphology and chemical composition of the synthesized $CuInSe_2$ films were studied by scanning electron microscopy (SEM LEO-1450), in the magnification range $\times 1000 \div \times 30000$ and resolution of 3.5 nm.

Electrophysical measurements of $CuInSe_2$ films were carried out at room temperature in the frequency range $\omega = 10^2 - 10^6$ Hz. The electrical resistance was measured using a four-contact method. A photoinduced change in resistance and impedance in a magnetic field was performed when the sample surface was illuminated between the contacts with a laser with a wavelength of 420 nm (blue). The duration of resistance measurement under illumination was $\sim 1$ min. The light flux power was maintained constant during the experiment.

## 3. Experimental findings and their discussion

The morphology of $CuInSe_2$ (CIS) films obtained by selenization strongly depends on the temperature of the selenization process, as it is a key parameter controlling reaction kinetics, element diffusion, and grain growth. All the films obtained were characterized by the absence of visible micro-punctures and good adhesion to the surface of glass substrates. The films contain microinclusions and conglomerates, which are three-dimensional regions of irregular shape closer to a quasi-spherical one (Figure 1).

With increasing reaction temperature $T_{sel} < 400\,^\circ C$ the microinclusions become larger and their number rises. At selenization temperatures $T_{sel} = 450 \div 550\,^\circ C$ the degradation of the film surface is observed, the microinclusions are diminished. On the surface of individual large conglomerates, the presence of micro voids (defects) is observed, probably related to the evaporation processes of the film material.

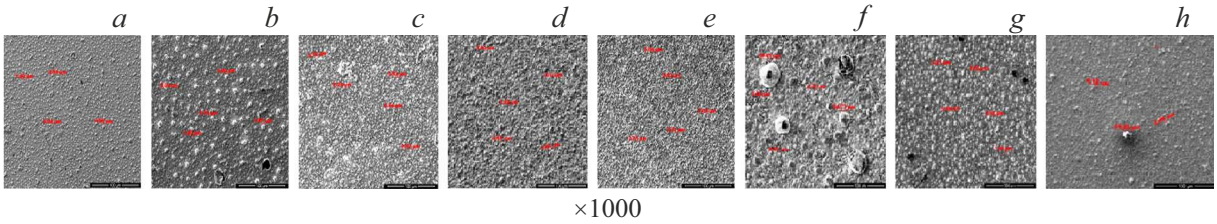


**Figure 1.** Morphology of the surface of $CuInSe_2$ films fabricated at selenization temperatures of $T_{sel} = 200\,^{\circ}C$ (*a*), $250\,^{\circ}C$ (*b*), $300\,^{\circ}C$ (*c*), $350\,^{\circ}C$ (*d*), $400\,^{\circ}C$ (*e*), $450\,^{\circ}C$ (*f*), $500\,^{\circ}C$ (*g*), $550\,^{\circ}C$ (*h*). Increase ×10.0 k.

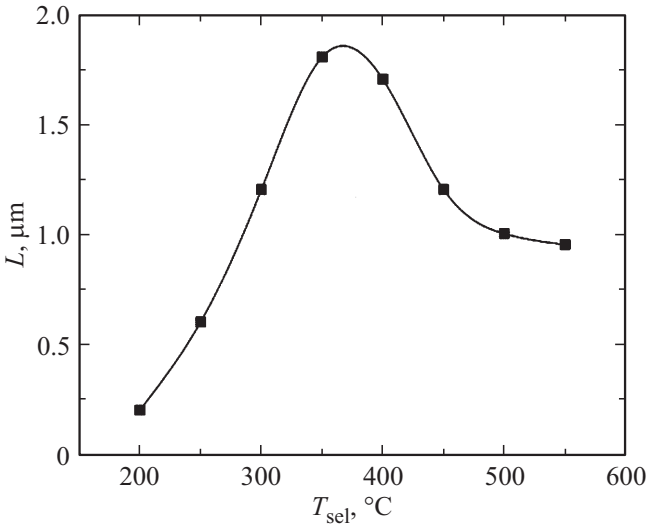


**Figure 2.** Average size of micro-inclusions versus selenization temperature in $CuInSe_2$ films.

The size distribution of the density of surface microinclusions obeys a lognormal law at $L > 0$:

$$f(L) = \frac{1}{L\sigma\sqrt{\pi}} \exp\left(-\frac{\ln^2(L/a)}{2\sigma^2}\right), \text{ where } f(L) \to \frac{n(L)}{S}, \quad (1)$$

where $a$ and $\sigma$ (average square, standard deviation) — parameters of lognormal distribution, $n(L)$ — number of micro-inclusions of size $L$, $S$ — film area, $f(L) = 0$ at $L \to 0$.

Figure 2 shows the curve of the average size of microinclusions versus temperature in $CuInSe_2$ films obtained at $T_{sel} = 200-550\,^{\circ}C$. By extrapolating the line to the temperature axis, we obtain the value of the minimum selenization temperature $T_{sel\,min} \approx 200\,^{\circ}C$, at which the formation of microinclusions can be observed. It should be noted that it was close to the temperature of $Cu_2Se$ formation.

Chemical analysis of the synthesized $CuInSe_2$ films showed that their composition is quasi-stoichiometric, and the distribution of components over the surface is uneven within (±3%). As the selenization temperature increases, the selenium concentration increases, and at $T_{sel} = 350 \div 400\,^{\circ}C$ the composition of the films is close to stoichiometric.

Figure 3 shows data from X-ray diffraction analysis of $CuInSe_2$ films obtained at selenization temperatures $T_{sel} = 200-550\,^{\circ}C$. The presence of a series of diffraction lines on the X-ray image suggests that the structure of the synthesized films is itself a chalcoperite structure (according to the standards file (Powder Diffraction File) from the International Center for Diffraction Data (ICDD) for $CuInSe_2$ PDF 00-040-1487). X-ray diffraction patterns of films obtained at selenization temperatures of $T_{sel} \geq 450^{\circ}C$

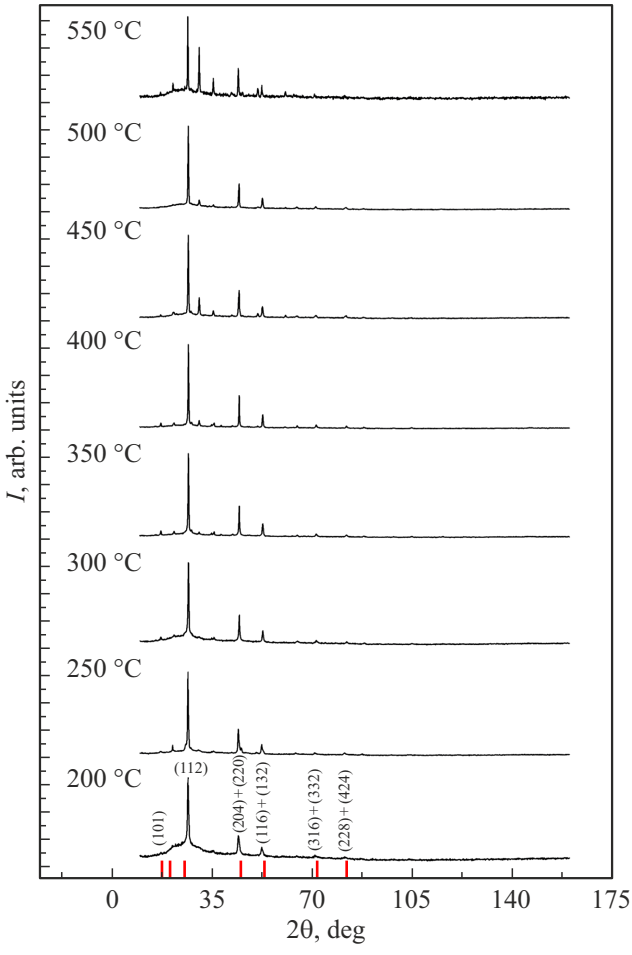


**Figure 3.** Data from X-ray diffraction analysis of polycrystalline $CuInSe_2$ films synthesized at different selenization temperatures

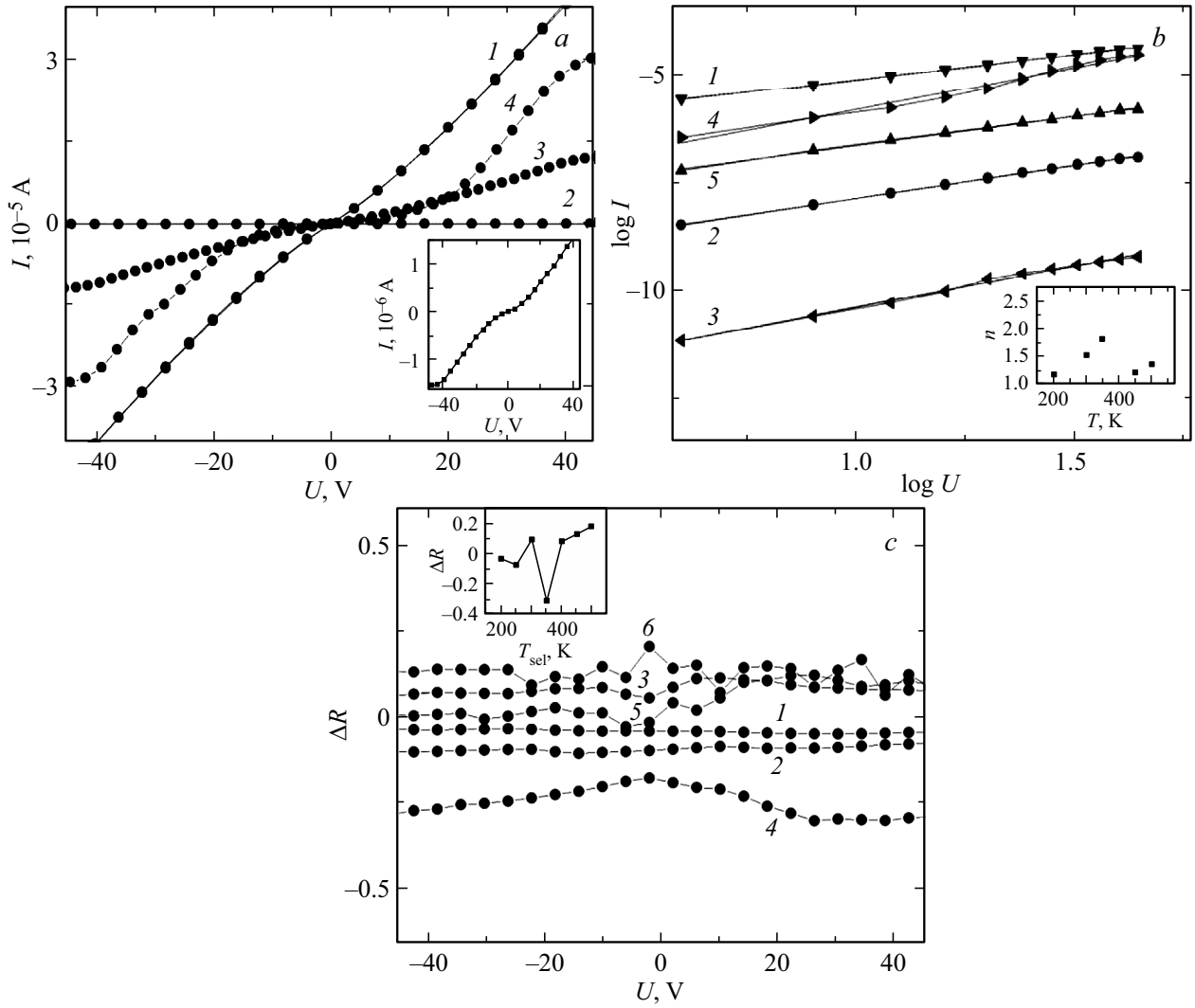


**Figure 4.** *a*) — Current-voltage curves of samples synthesized at $T_{sel} = 200\,^{\circ}$C (*1*); 250 °C (*2*); 350 °C (*3*); 400 °C (*4*). The insert window in Figure 4, *a* shows the current-voltage curve for the samples $T_{sel} = 500\,^{\circ}$C. (*b*) — The current-voltage curves in the logarithmic scale for the samples $T_{sel} = 200\,^{\circ}$C (*1*); 300 °C (*2*); 350 °C (*3*); 400 °C (*4*); 500 °C (*5*). In the insert window, the dependence of the degree of electrical heterogeneity on the selenization temperature. (*c*) — relative change of resistance $\Delta R = R(\text{light}) - R(0)/R(0)$ when exposed to light $R(\text{light})$ and with no light $R(0)$ versus voltage of samples synthesized at $T_{sel} = 200\,^{\circ}$C (*1*); 250 °C (*2*); 300 °C (*3*); 350 °C (*4*); 400 °C (*5*); 500 °C (*6*). The insert in Figure 4, *c* shows $\Delta R$ versus $T_{sel}$ for $CuInSe_2$ film.

revealed the presence of additional bands, probably associated with the compound $Cu_{1-x}Se_x$.

Let's analyze how these facts affect photoconductivity and photoinduced changes in impedance, knowing that in photoconductivity, grain size and defects affect the lifetime of carriers. For impedance, grain boundaries and porosity change the resistance and capacitance components.

The current-voltage curve (I-V) can provide information about the degree of electrical heterogeneity. In films with an electrically inhomogeneous charge distribution, the I-V is described by the Mott or Poole–Frenkel law [22]. As the selenization temperature of films increases to 350 °C, the resistance increases and reaches a maximum for films synthesized at 350 °C. The behavior of the I-V is symmetrical and nonlinear (Figure 4, *a*). The current versus voltage is delineated by a power function $I = AU^n$, where power exponent $n$ grows from $n = 1.2$ ($T_{sel} = 200\,^{\circ}$C) to $n = 1.5$ ($T_{sel} = 300\,^{\circ}$C) and at $T_{sel} = 500\,^{\circ}$C $n = 1.4$ (Figure 4, *b*, insert window Figure 4, *b*). At $T = 350\,^{\circ}$C the films are better described by Mott's law, i. e., there is a spatial volume charge in the films. A further increase in the selenization temperature leads to higher conductivity and lower nonlinearity of the current-voltage curves.

Figure 4, *c* illustrates the relative change of resistance $\Delta R = R(\text{light}) - R(0)/R(0)$ versus voltage when the samples are exposed to light $R(\text{light})$ and not exposed to light $R(0)$. This figure confirms the dependence of photoconductivity on the selenization temperature. For samples synthesized at $T\text{sel} = 200\,^{\circ}$C, 250 °C and 350 °C, the resistance decreases under illumination and reaches its

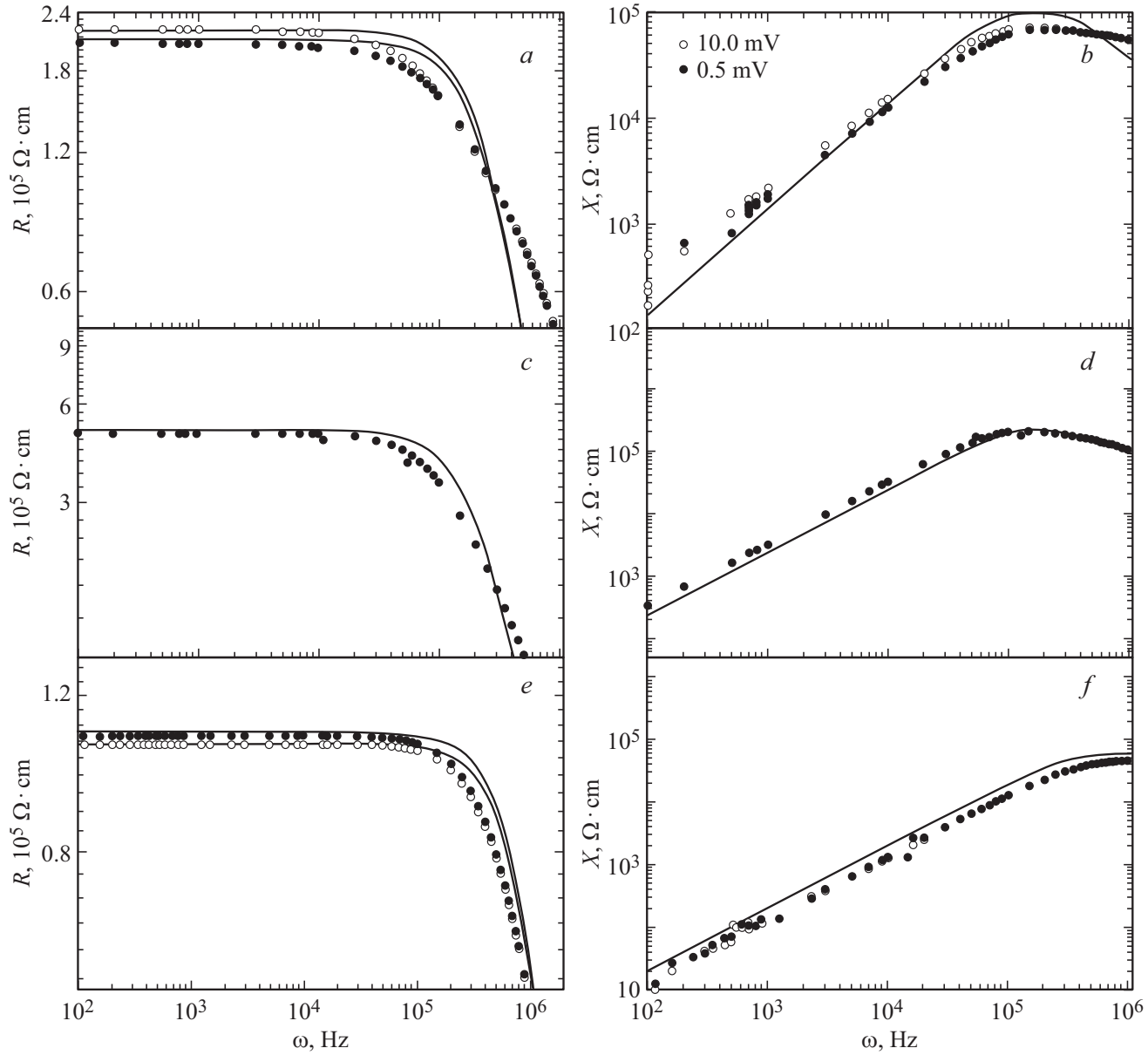


**Figure 5.** Frequency dependences of the real and imaginary parts of the impedance of samples obtained at $T_{sel} = 200$ K (*a, b*); 250 K (*c, d*); 400 (*e, f*). The adjustable functions of the Debye equation are marked by solid lines.

maximum effect on a film synthesized at $T_{sel} = 350\,^{\circ}$C. According to the morphological analysis data, films have a maximum grain size at this temperature and the synthesis condition at this selenization temperature is optimal for the fabrication of films with maximum photoelectric effect.

For $CuInSe_2$ films synthesized at $T_{sel} > 350\,^{\circ}$C resistance grows with lighting. Perhaps, when illuminated above this temperature, the average mobility of electrons and holes changes. At $T_{sel} < 400\,^{\circ}$C the mobility of electrons, which experience elastic scattering on a negative spatial charge, prevails, the mobility of holes is significantly less than that of electrons. As a result, the holes shield the negative charge. At high temperatures, the concentration of defects rises, according to microstructural analysis data. Electrons and holes induced by photon absorption are pinned on these defects, which results in the formation of charged regions and causes additional scattering of current carriers. A change in the charge state of a defect can significantly affect its ability to dissipate the main current carriers. Either this is due to a change in the charge state of defects at grain boundaries or on the film surface when exposed to light, which increases the height of barriers under light exposure and makes it difficult for current carriers to pass between the grains.

In addition to the fact that the samples contain many defects in the form of traps and vacancies, they are also electrically inhomogeneous. Figure 5 illustrates the frequency dependencies of real $Z'$ (ohmic resistance $R$)

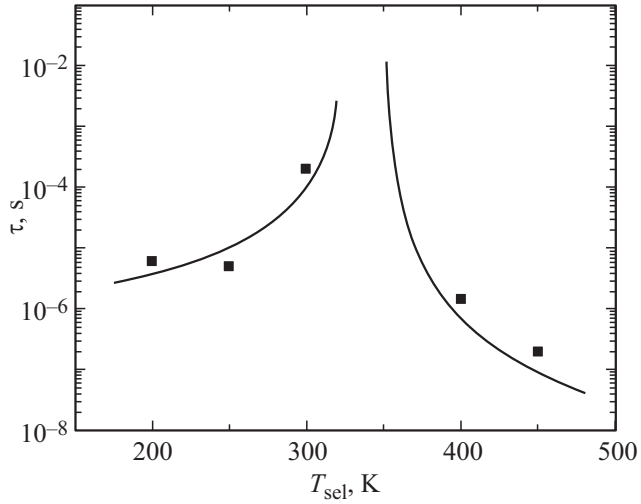


**Figure 6.** Relaxation time versus selenization temperature. Adjustable power functions are marked with solid lines.

and imaginary $Z''$ (reactance $X$) part of the impedance. An increase in selenization temperature $T_{sel}$ leads to higher values of the impedance components up to 350 °C.

Relaxation time is a key parameter determining the efficiency of semiconductor materials for applications based on photoconductivity: solar cells, photodetectors, photoconductive cells, and optical sensors. The frequency dependence of the impedance components is described in Debye model:

$$R(\omega) = \frac{A}{1 + (\omega\tau)^2}; \quad X(\omega) = \frac{B\omega\tau}{1 + (\omega\tau)^2}, \qquad (2)$$

where $A$ and $B$ — parameters which remain constant and do not depend on temperature, and $\tau$ — current carriers relaxation time.

Figure 6 shows relaxation time versus selenization temperature for $CuInSe_2$ samples, which is satisfactorily described by a power function: $\tau = A/(T - 350\,\mathrm{K})^2$ at $T < 350\,\mathrm{K}$ and $\tau = B/(T - 350\,\mathrm{K})^3$ at $T_{sel} > 350\,\mathrm{K}$.

The relaxation of charge carriers in $CuInSe_2$ films may be an experimental evidence of their complex and inhomogeneous electronic structure, with many defects and grain boundaries that directly depend on the processing temperature. The dependence of the relaxation time on the selenization temperature can be used as a method for determining high-quality films with minimal defective structure and with a photoelectric effect. The relaxation time ($\tau$) reaches the maximum value for the film synthesized at $T_{sel} = 350\,^\circ\mathrm{C}$, and exceeds the limits of the instrument measurements. In this temperature range, the maximum nonlinearity of I-V and the maximum value of the photocurrent are reached. The photogenerated holes shield the spatial charge, as a result, the mobility of electrons increases.

The impedance rises with increasing selenization temperature, passes through a maximum at 350 °C and plummets with further heating (Figure 7).

A study of photoinduced changes of impedance $\Delta Z = Z(\mathrm{light}) - Z(0)/Z(0)$ under the action of light $Z(\mathrm{light})$ and without light $Z(0)$ for $CuInSe_2$ samples synthesized at different selenization temperatures showed no effect in the temperature range $T_{sel} = 300-550\,^\circ\mathrm{C}$ (Figure 8). A promising direction is the synthesis of samples at 200 °C and 250 °C, since the maximum effect of $\Delta Z$ was found on samples synthesized at these temperatures. At $T_{sel} = 200$ and 250 °C the impedance goes down during lighting $\Delta Z$ by 5–8 % (Figure 8). The selenization temperature plays

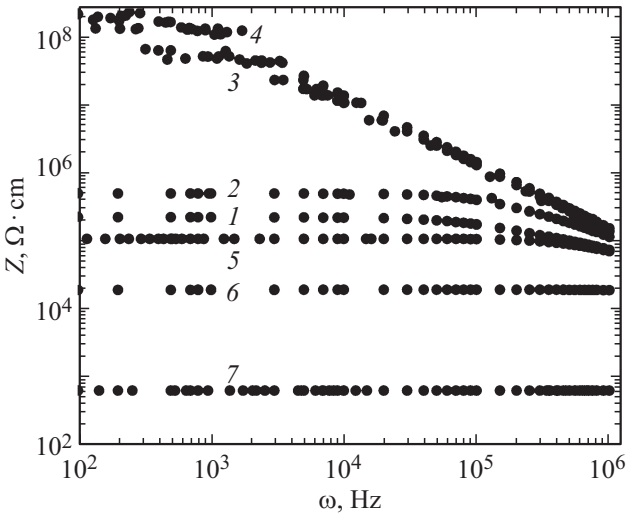


**Figure 7.** Frequency dependences of the impedance at different selenization temperatures 200 °C (*1*); 250 °C (*2*); 300 °C (*3*); 350 °C (*4*); 400 °C (*5*); 450 °C (*6*); 550 °C (*7*).

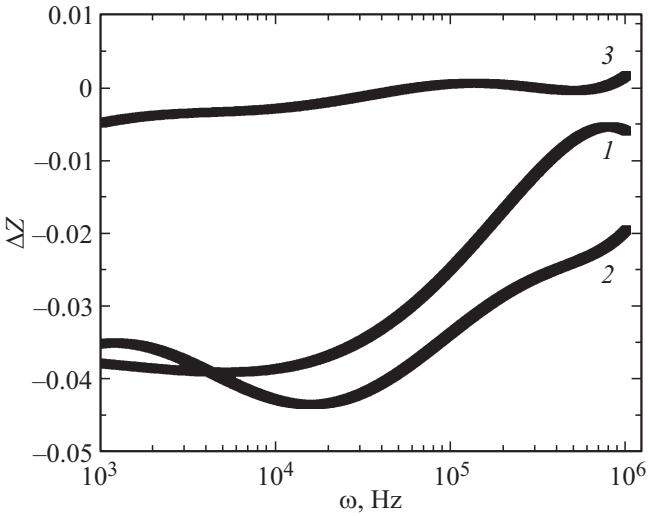


**Figure 8.** Frequency dependencies of impedance variation $\Delta Z = Z(\mathrm{light}) - Z(0)/Z(0)$ when exposed to light $Z(\mathrm{light})$ and with no light $Z(0)$ for the samples synthesized at $T_{sel} = 200\,\mathrm{K}$ (*1*); 250 K (*2*); 300 K (*3*)

the role of an activator of the process. Selenium depletion of the film will result in excess of copper and indium.

Therefore, photoeffects can be dubbed an indicator of synthesis quality. These methods make it possible to optimize the synthesis process by selecting conditions that maximize the desired optoelectronic properties of a future device. In the synthesis of solar cells, it is useful to study the fundamental role of defects in CIS.

## 4. Conclusions

$CuInSe_2$ films with chalcoperite crystal structure were obtained by controlled selenization. Analysis of the data obtained showed that the selenization temperature is a critical parameter for controlling the morphology of CIS films. The films exhibit a nonlinear I-V, which is associated with electrical inhomogeneity. Analysis of I-V of films synthesized at 350 °C showed that the dependence $I(U)$ is described by Mott's law and the presence of a volumetric spatial charge in them. The optimal selenization temperature of films with the maximum value of photoelectric effect and with the maximum value of relaxation time has been identified. Lowering of selenization temperature $T_{sel} \leq 300$ °C causes a photoinduced change in impedance.

### Acknowledgments

The study was carried out within the framework of the research topic of the State Assignment of the Institute of Physics of the Siberian Branch of the Russian Academy of Sciences.

### Conflict of interest

The authors declare that they have no conflict of interest.

## References

[1] T. Nakada, K. Migita, A. Kunioka. Jpn. J. Appl. Phys. **32**, L1169 (1993). DOI: 10.1143/jjap.32.l1169
[2] E.P. Zaretskaya, V.F. Gremenyuk, V.B. Zalessky, V.A. Ivanov, I.V. Viktorov, V.I. Kovalevsky, O.V. Ermakov, T.R. Leonova. ZhTF **70**, 141 (2000). (in Russian).
[3] J. Ramanujam, U.P. Singh. Energy Environ.Sci. **10**, 1306 (2017). DOI: 10.1039/C7EE00826K
[4] X. Liu, Y. Feng, H. Cui, F. Liu, X. Hao, G. Conibeer, D.B. Mitzi, M. Green. Prog. Photovolt. **24**, 879 (2016). DOI: 10.1002/pip.2741
[5] J.L. Shay, J.H. Wernick. Ternary Chalcopyrite Semiconductors: Growth, Electronic Properties, and Applications. Pergamon, Press (1975). 244 p.
[6] P. Jackson, R. Wuerz, D. Hariskos, E. Lotter, W. Witte, M. Powalla. Phys. Stat. Sol. Rapid Res. Lett. **10**, 583 (2016). DOI: 10.1002/pssr.201600199
[7] M. Jamiati. JITL **4**, 365 (2021). DOI: 10.22051/JITL.2022.35435.1051
[8] S. Lany, A. Zunger. Phys. Rev. B **78**, 235104 (2008). DOI: 10.1103/PhysRevB.72.035215
[9] S. B. Zhang, S.H. Wei, A. Zunger, H. Katayama-Yoshida. Phys. Rev. B **57**, 9642 (1998). DOI: 10.1103/PhysRevB.57.9642
[10] J.M. Cho, E.J. Bae, J.D. Suh, K.B. Song. J. Nanoelectron. Optoe. **5**, 218 (2010). DOI: 10.1166/jno.2010.1097
[11] A. Rockett, R. W. Birkmire. J. Appl. Phys. **70**, R81 (1991). DOI: 10.1063/1.349175
[12] M. Igalson, H. W. Schock. J. Appl. Phys. **80**, 5765 (1996). DOI: 10.1063/1.363631
[13] D. Schmid, M. Ruckh, F. Grunwald, H.W. Schock. J. Appl. Phys. **73**, 2902. (1993). DOI: 10.1063/1.353020
[14] A. Zakery, S.R. Elliott. J. Non-Cryst. Solids **330**, 1 (2003). DOI: 10.1016/j.jnoncrysol.2003.08.064
[15] U. Rau, J.H. Werner. Appl. Phys. Lett. **84**, 3735 (2004). DOI: 10.1063/1.1737071
[16] T. Feurer, P. Reinhard, E. Avancini, B. Bissig, J. Löckinger, P. Fuchs, R. Carron, T. P. Weiss, J. Perrenoud, S. Stutterheim, S. Buecheler, A.N. Tiwari. Prog. Photovolt. **25**, 645 (2017). DOI: 10.1002/PIP.2811
[17] S. Ouédraogo, M.B. Kébré, A.T. Ngoupo, D. Oubda, F. Zoumoré, J.-M. Ndjaka. AMPC **10**, 151 (2020). DOI: 10.4236/AMPC.2020.107011
[18] S. Mandati, B.V. Sarada, S.R. Dey, S.V. Joshi. Semiconductors-Growth and Characterization / Edited by R. Inguanta and C. Sunseri (2018). DOI: 10.5772/intechopen.71857
[19] M.R. Pallavolu, R.R. Nallapureddy, H.R. Barai, S.W. Joo. Thin Solid Films **709**, 138238 (2020). DOI: 10.1016/j.tsf.2020.138238
[20] G.M. Mikhailov, I.V. Malikov, A.V. Chernykh, V.T. Petrashov. Thin Solid Films **293**, 315 (1997). DOI: 10.1016/S0040-6090(96)08953-5
[21] G. Regmi, S. Velumani. Mat. Sci. Semicond. **137**, 106215 (2022) DOI: 10.1016/j.mssp.2021.106215
[22] N.F. Mott, E.F. Davis. Electronic Processes in Non-Crystalline Materials. Clarendon Press, Oxford (1971). 438 p.

*Translated by T.Zorina*